Discovery of Giant Unit-Cell Super-Structure in the Infinite-Layer Nickelate PrNiO$_2$

J. Oppliger,[1, *] J. Küspert,[1] A.-C. Dippel,[2] M. v. Zimmermann,[2] O. Gutowski,[2] X. Ren,[3, 4]
X. J. Zhou,[3] Z. Zhu,[3] R. Frison,[1] Q. Wang,[1, 5] L. Martinelli,[1] I. Biało,[1] and J. Chang[1, †]

[1]*Physik-Institut, Universität Zürich, Winterthurerstrasse 190, CH-8057 Zürich, Switzerland*
[2]*Deutsches Elektronen-Synchrotron DESY, Notkestraße 85, 22607 Hamburg, Germany.*
[3]*Beijing National Laboratory for Condensed Matter Physics,
Institute of Physics, Chinese Academy of Sciences, Beijing 100190, China*
[4]*School of Physical Sciences, University of Chinese Academy of Sciences, Beijing 100049, China*
[5]*Department of Physics, The Chinese University of Hong Kong, Shatin, Hong Kong, China*

Spectacular quantum phenomena such as superconductivity often emerge in flat-band systems where Coulomb interactions overpower electron kinetics. Engineering strategies for flat-band physics is therefore of great importance. Here, using high-energy grazing-incidence x-ray diffraction, we demonstrate how *in-situ* temperature annealing of the infinite-layer nickelate PrNiO$_2$ induces a giant superlattice structure. The annealing effect has a maximum well above room temperature. By covering a large scattering volume, we show a rare period-six in-plane (bi-axial) symmetry and a period-four symmetry in the out-of-plane direction. This giant unit-cell superstructure likely stems from ordering of diffusive oxygen. The stability of this superlattice structure suggests a connection to an energetically favorable electronic state of matter. As such, our study provides a new pathway – different from Moiré structures – to ultra-small Brillouin zone electronics.

Applications of transition metal oxides span from dental restoration to high-tech semiconductor devices [1]. At the same time, oxide materials host some of the most enigmatic phases of quantum matter. For example, high-temperature superconductivity in the cuprates (copper-oxides) is still an active field of research [2]. A longstanding challenge is to – by design – realize cuprate-physics in other materials [3]. Low-valence nickelates have been a prime candidate for this task. The discovery of superconductivity in doped La$_{1-x}$Sr$_x$NiO$_2$ therefore sparked immediate excitement [4–8]. Much of the following experimental work has been discussed with cuprate physics as reference [9–11]. Experimental studies and calculations agree on a dominant $3d^{9-\delta}$ ground state, but highlighted important differences with respect to cuprates, including a more prominent Mott-Hubbard gap and an active role of rare-earth bands at the Fermi level [9, 11–13].

Similarities were strengthened by the discovery of dispersive magnon excitations, revealing strong antiferro-magnetic exchange [14, 15]. A crucial characteristics of cuprates is the presence of two-dimensional charge order in the superconducting planes. Such modulation, ubiquitous both in hole [16–18] and electron-doped cuprates [19], seems to be a rather fundamental property of the two-dimensional Hubbard model [20, 21]. Therefore, great experimental effort has been put in the search of a similar broken symmetry in nickelates. Recently, the presence of a charge modulation along Ni-O bonds, was discovered in La-, Nd- and Pr-based nickelates by resonant x-ray scattering [15, 22–25]. However, the interpretation of these results in terms of charge order is surrounded by controversy [26, 27]. Unlike in cuprates, the order lacks a clear temperature dependence [15, 23]. Moreover, its dependence on sample preparation [23] and the unclear role of an epitaxial capping layer [15] question its universality in the family of nickelates. Other proposals to explain the observed modulation include the formation of hydrogen chains [28] or superstructure of re-intercalated oxygen atoms [29].

Here we present a high-energy, grazing-incidence x-ray diffraction study of PrNiO$_2$ with crystalline and amorphous SrTiO$_3$ (STO) capping layer. In contrast to resonant diffraction, this technique covers a large scattering volume across many Brillouin zones. Our main finding is a stable, giant unit cell emerging upon *in-situ* thermal heating above ambient temperature. In the NiO$_2$ plane, a rare period-six translational symmetry occurs with a period-four stacking order in the out-of-plane direction. This giant unit-cell superstructure remains stable over a large temperature range and emerges irrespectively of crystalline or amorphous capping. As such, it represents a fundamentally novel structure – most likely originating from ordering of diffusive oxygen. Quenching this structure to low-temperature promises access to new ultra-small Brillouin zone electronics.

RESULTS

Our grazing-incidence diffraction geometry is schematically illustrated in the lower part of Fig. 1(a). By rotating the sample around the direction perpendicular to the scattering plane, a three-dimensional scattering volume is collected. As exemplified by data on a PrNiO$_2$ thin film grown on an STO substrate with crystalline

---

[*] jens.oppliger@physik.uzh.ch
[†] johan.chang@physik.uzh.ch
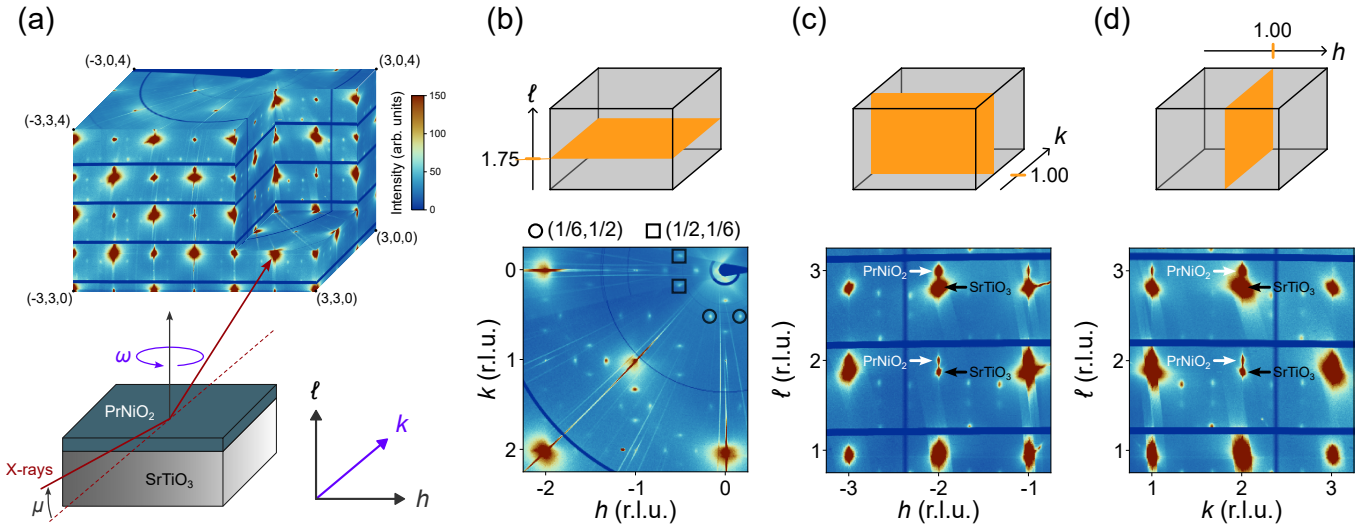
FIG. 1. **High-energy grazing-incidence x-ray diffraction on a PrNiO$_2$ thin film.** (a) Schematic illustration of diffraction geometry. A three-dimensional scattering volume is recorded by high-energy grazing-incidence (angle μ) x-rays, diffracted on a horizontal film, which is rotated around its vertical axis (ω). (b-d) Two-dimensional cuts displayed schematically (top) together with intensity maps of respectively the $(h, k, 1.75)$, $(h, 1, \ell)$ and $(1, k, \ell)$ scattering planes measured at 386 K (bottom). Diffracted intensities are visualized using a linear false color scale. Fundamental Bragg reflections of the PrNiO$_2$ film and the SrTiO$_3$ (STO) substrate are indicated by arrows in (c) and (d). Principle superlattice reflections are highlighted with square and circular symbols in (b).

STO capping layer, this scattering volume (h, k, ℓ) covers dozens of Brillouin zones as shown in the upper part of Fig. 1(a). In Fig. 1(b-d), we display two-dimensional slices of the scattering volume. From such slices, fundamental Bragg reflections yield information about lattice parameters and translational symmetry breaking. As common for expitaxially strained growth, the in-plane lattice parameters of PrNiO$_2$ and the STO substrate are identical within our experimental resolution (see Table I of the methods section). By contrast, along the out-of-plane c-axis direction, lattice parameters of substrate and the PrNiO$_2$ film are clearly different – see Fig. 1(c,d).

We find that fundamental Bragg peaks at $\tau = (h_B, k_B, \ell_B)$ – with h_B, k_B, and ℓ_B being integers – are virtually temperature independent. Upon heating above room temperature, we discover the emergence of additional commensurate reflections. These reflections occur at $Q_o = \tau q_o^i$ with

$$q_o^{a,b} = (\delta_h, \delta_k, 0) \quad \text{and} \quad q_o^c = (0, 0, \delta_\ell) \qquad (1)$$

and in-plane commensurabilities $\delta_h \approx \delta_k \approx 1/6$ and out-of-plane commensurability $\delta_\ell \approx 1/4$. Examples of superlattice peaks at $Q_o = (\pm 1/6, 1/2, 7/4)$ and $Q_o = (1/2, \pm 1/6, 7/4)$ are highlighted by circles and squares in Fig. 1(b). Notice that the $Q_o = (1/6, 1/6, \ell_B \delta_\ell)$ reflection is either weak or symmetry forbidden.

In Fig. 2, we focus on the $(h, 1/2, \ell)$ and $(h, 1, \ell)$ scattering planes respectively for a PrNiO$_2$ thin film with crystalline STO capping layer – see Supplementary Fig. S1 for equivalent $(1/2, k, \ell)$ and $(1, k, \ell)$ data.

Reflections in both scattering planes display the same temperature dependence. Initially, the superlattice peaks emerge and are enhanced upon heating above room temperature. Note that at room temperature, the out-of-plane scan reveals a broad peak centred around $\delta_\ell \approx 1/3$ – see Fig. 2(f). This is also in agreement with previous resonant x-ray scattering studies [23, 24, 27]. Upon heating, the out-of-plane commensuration changes to a sharp peak with $\delta_\ell \approx 1/4$ as shown in Fig. 2(c,f). This phase with quarter commensuration furthermore displays a much longer out-of-plane correlation length ξ_c, indicating an improved stacking order. The PrNiO$_2$ film with amorphous capping does not display any ordering at room temperature. For this system, the superlattice structure emerges only at higher temperatures first with $\delta_h \approx \delta_k \approx 1/6$ and a broad peak with $\delta_\ell \approx 1/3$. At even higher temperatures the out-of-plane commensuration – like in the case of crystalline capping – manifests as a sharp peak with $\delta_\ell \approx 1/4$.

In Fig. 3, we summarize the temperature dependence of the superlattice peaks for systems with crystalline and amorphous STO capping layer. Fig. 3(a,b) shows that the PrNiO$_2$ in-plane (a, b) lattice constants are essentially temperature independent. By contrast, the c-axis lattice constant shows a step-like temperature dependence – see Fig. 3(c). Roughly at this step (highlighted with arrows), the quartet peaks at Q_o appear. For temperatures above 600 K these peaks are suppressed and eventually vanish at temperatures above 800 K as shown in Fig. 3(d). High enough temperatures therefore seem to reverse the topotactic reaction and return the film system to the PrNiO$_3$ cubic perovskite structure. This is con-
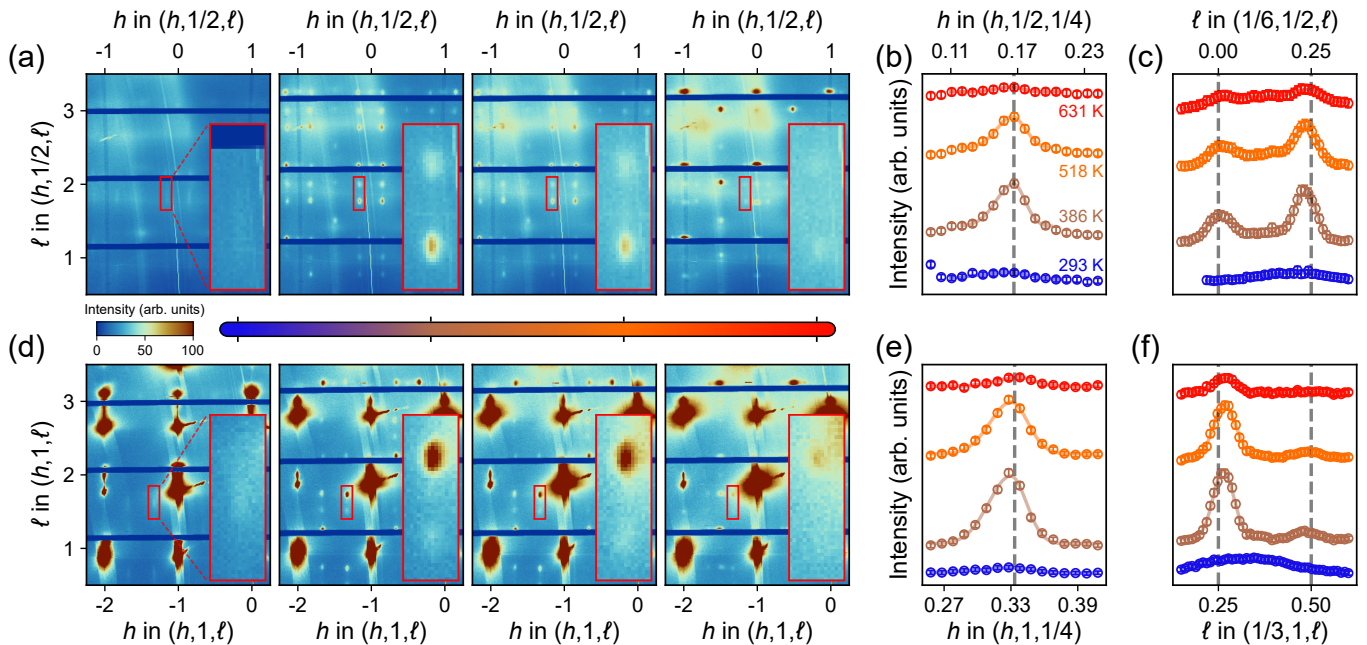
FIG. 2. **Thermal-induced superlattice structure in a PrNiO₂ thin film.** (a,d) Diffraction intensities (linear false color scale) in the $(h, 1/2, \ell)$ and $(h, 1, \ell)$ scattering planes as a function of temperature. The four temperatures are indicated in panel (b). The most intense peaks stem from fundamental Bragg peaks of the STO substrate and the PrNiO₂ thin film. Selected superlattice peaks are highlighted by the red rectangular boxes. (b,c) One-dimensional h (in-plane) and ℓ (out-of-plane) scans through the superlattice reflections in (a) for temperatures as indicated. (e,f) Equivalent h and ℓ scans but through the superlattice reflections in (d). Solid lines are Gaussian profiled fits with a sloping background. Error bars reflect counting statistics.

firmed by laboratory 2θ scans shown in Supplementary Fig. S2. These trends are observed both for films with crystalline and amorphous capping. For the sample with amorphous capping, the onset temperature of the quartet peaks is shifted by around 100 K and is less pronounced compared to the sample with crystalline capping. Interestingly, the in-plane $\delta_h \approx \delta_k \approx 1/6$ and out-of-plane $\delta_\ell \approx 1/4$ commensurations show little to no temperature dependence – see Fig. 3(e). Similarly, both in-plane and out-of-plane correlation lengths – shown in Fig. 3(f) – plateau in the ordered state.

DISCUSSION

We summarize our results using a schematic diagram in Fig. 4. Between the known ANiO₂ and ANiO₃ crystal structures, there exist – at least two – superlattice structures with gigantic unit cells. The superlattices are composed of two independent orderings: A fundamental two-dimensional ordering and different stacking patterns. This is reminiscent of two-dimensional charge orderings in the cuprates or dichalcogenides where different stacking orders frequently occur. In our particular case, we report a fundamental in-plane order that stacks with a (short-range) period three or a (long-range) period four along the c-axis. Based on our diffraction experiment, it is not possible to distinguish checkerboard (biaxial) from

twinned stripe order.

Irrespective of exact symmetry breaking, the reflections contain valuable information about the nature of the ordering. The observed superlattice reflections are intense – only one or two orders of magnitude weaker than the fundamental Bragg peaks of the thin film (see Fig. 1). This suggests that the symmetry breaking stems from a strong ordering tendency [30]. This would be atypical for charge density waves that typically manifest by weak reflections. Yet, both electronic or atomistic driven mechanisms are possible.

The fact that the ordering can be quenched (see Supplementary Fig. S3), suggests that the observed symmetry breaking goes beyond a standard crystal structure phase transition. It is possible that oxygen diffuses from the substrate and/or capping layer to the PrNiO₂ film or that the topotactic process resulted in a residual apical oxygen occupation. High temperatures will enhance oxygen diffusion and promote an oxygen annealing process as seen for example in YBa₂Cu₃O₆₊ₓ [31]. Oxygen diffusion would render our PrNiO₂ film off-integer stochiometric by occupying vacant apical oxygen positions. Such a partial apical oxygen occupation is consistent with the observed c-axis extension – see Fig. 3(c). A single apical oxygen atom per 6x6x4 (original) unit cells generates the observed symmetry breaking. As such, the reported superlattice structure is closely related to the ANiO₂ composition.
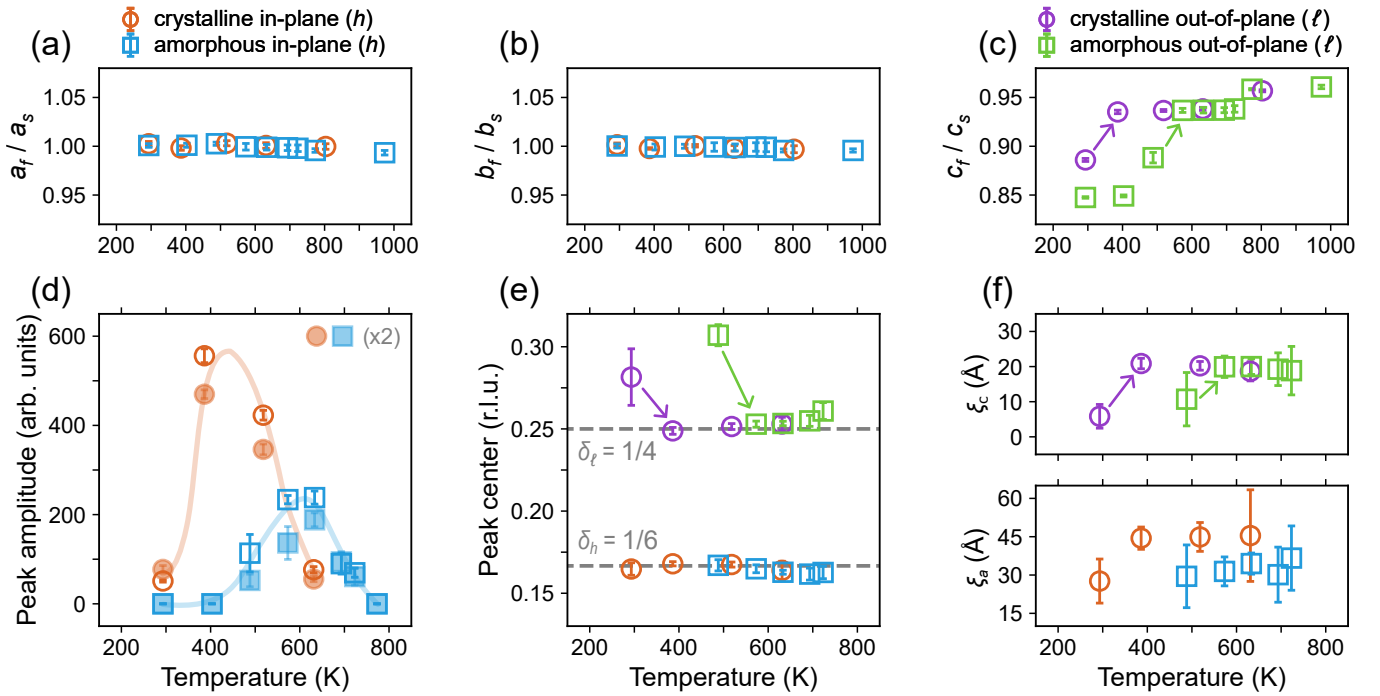
FIG. 3. **Temperature and capping layer dependence of the superlattice structure.** (a-c) PrNiO$_2$ thin film lattice constants x_f – normalized to the STO substrate lattice constants x_s, with $x = a, b, c$ for films with crystalline and amorphous capping layers. (d) Peak amplitude versus temperature of selected reflections $Q_o = (1/6, 1/2, 7/4)$ (filled markers) and $Q_o = (1/3, 1, 7/4)$ (empty markers) for films with crystalline and amorphous STO capping. Amplitude of $Q_o = (1/6, 1/2, 7/4)$ has been scaled by a factor of two. Solid lines are guides to the eye. (e) In-plane δ_h and out-of-plane δ_ℓ commensuration plotted versus temperature. (f) In-plane ξ_a and out-of-plane ξ_c correlation lengths versus temperature. Data in (e) and (f) is averaged over the two reflections separately for crystalline and amorphous capping. Error bars represent one standard deviation obtained from a least squares fitting procedure.

We stress that due to the weak form factor, apical (or in-plane) oxygen alone can not explain the observed structure factor. However, apical oxygen inclusions may induce Ni and Pr distortion patterns. Due to the large atomic mass, Pr distortions are likely to dominate the structure factor. A structural refinement would be an interesting future extension of this work.

An open pressing question is as to why the giant 6x6x4 unit cell manifests over a 300 K temperature range, irrespective of crystalline or amorphous capping. In principle, oxygen diffusion would produce an arbitrary oxygen stochiometry. Our observation of a stable giant superstructure implies a significant down-scaling of the Brillouin zone. This in turn induces massive band folding that often generates flat band physics as for example seen in magic-angle twisted bilayer graphene [32]. As such, it is possible that the superstructure induces an electronic state with favorable energetics. This hypothesis therefore implies the existence of two fundamentally different ground states of PrNiO$_{2+x}$. The fact that spin excitations – in ANiO$_2$ – are not observed in combination with this symmetry breaking [15], supports this rationale. It would thus be of great interest to quench the giant superlattice structure to low temperature for studies of its electronic structure and properties.
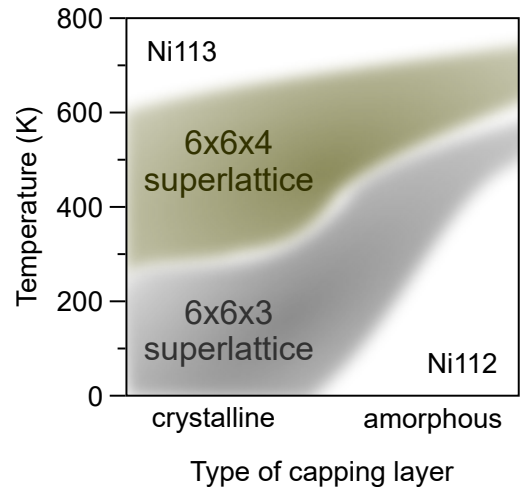
FIG. 4. **Schematic "phase" diagram of ANiO$_{3-x}$.** Through a topotactic reduction, ANiO$_3$ (Ni113) films can be oxygen reduced to stochiometric ANiO$_2$ (Ni112) that upon hole doping displays superconductivity. Our study suggests that oxygen diffusion can stabilize a 6x6x4 superstructure. The diffusion process can be accelerated by annealing the thin film. At high enough temperatures, the system will return to the ANiO$_{3-x}$ oxygen stochiometry.

METHODS

Film systems: Two different capped films of $PrNiO_2$ on a $SrTiO_3$ (STO) substrate have been studied. Thicknesses of films and cappings are indicated in Table I along with lattice parameters. The thin films were grown on a (001)-oriented $SrTiO_3$ substrate by pulsed laser deposition. During growth, the substrate temperature was kept at 600 °C under an oxygen partial pressure of 150 mTorr. After topotactic reduction (390 °C for 2 h), the pervoskite phase is transformed into an infinite-layer phase. The dimensions of both samples are $5 \times 5 \times 0.5$ mm^3. Both samples were cleaned with isopropyl and afterwards dried with compressed air. Prior to the measurement the thin film with crystalline capping was exposed to air for over a day. The thin film with amorphous capping was measured immediately after it has been removed from an inert atmosphere.

TABLE I. **Studied film systems.** Lattice parameters and thicknesses of the two capped film systems used for this study. In-plane parameters of the substrate, film and capping are identical within the experimental sensitivity. Given that the capping layer is very thin, it is not possible to identify the c-axis lattice parameter and hence this entry is indicated by $\varnothing$. Use of amorphous STO capping yields a c-axis lattice parameter comparable to cap-free $PrNiO_2$ films [6, 33].

Film system	Thickness [nm]	a [Å]	b [Å]	c [Å]
Cryst. STO capping	4.0			$\varnothing$
$PrNiO_2$	7.0	3.885	3.905	3.450
STO substrate	∞			3.895
Amorph. STO capping	5.0			$\varnothing$
$PrNiO_2$	7.6	3.900	3.915	3.305
STO substrate	∞			3.900

Diffraction experiments: High energy x-ray diffraction experiments were carried out at the second experimental hutch (EH2) of the P07 beamline [34–36] at the PETRA III storage ring (DESY, Hamburg). 73 keV x-rays with grazing-incidence geometry ($\mu = 0.05°$) and a Detectris Pilatus3 X CdTe 2M detector were used. For each scan, an angular range of 200° (ω in Fig. 1(a)) has been covered using a total of 2000 frames. Each frame therefore corresponds to an angular range of 0.1°. The exposure time per frame was set to 0.05 s. Temperature was controlled by a resistive heating plate and the sample was kept in a helium atmosphere with constant flow rate.

Data analysis: Detector images are reconstructed into reciprocal space and shown two-dimensional data slices are integrated over 0.1 reciprocal lattice units (r.l.u.) along the slicing direction. The peaks of the one-dimensional line profiles for the sample with (crystalline) amorphous capping layer are fitted with a (linear) quadratic background and a (split) Gaussian function. Correlation lengths when using a split Gaussian function are obtained from the average of the standard deviations of the Gaussians.

Data availability. All experimental data are available upon reasonable request to the corresponding authors.

Author contributions: X.R., X.J.Z. and Z.Z. grew the $PrNiO_2$ films. Sample preparation for the x-ray experiments were organized by I.B. and J.K.. J.O., J.K., O.G., A.C.D., M.v.Z., and J.C. carried out the experiment. J.O. carried out the data analysis with assistance from M.v.Z., J.K., I.B., L.M., and J.C. The project was conceived by Q.W. and the manuscript was written by J.O. and J.C. with assistance from all authors. J.O. and J.K. contributed equally.

Competing interests: The authors declare no competing interests.

[1] J. Shi, J. Zhang, L. Yang, M. Qu, D.-C. Qi, and K. H. L. Zhang, "Wide bandgap oxide semiconductors: from materials physics to optoelectronic devices," Advanced Materials **33** (2021), 10.1002/adma.202006230.

[2] B. Keimer, S. A. Kivelson, M. R. Norman, S. Uchida, and J. Zaanen, "From quantum matter to high-temperature superconductivity in copper oxides," Nature **518**, 179–186 (2015).

[3] M R Norman, "Materials design for new superconductors," Reports on Progress in Physics **79**, 074502 (2016).

[4] D. Li, K. Lee, B. Y. Wang, M. Osada, S. Crossley, H. R. Lee, Y. Cui, Y. Hikita, and H. Y. Hwang, "Superconductivity in an infinite-layer nickelate," Nature **572**, 624–627 (2019).

[5] D. Li, B. Y. Wang, K. Lee, S. P. Harvey, M. Osada, B. H. Goodge, L. F. Kourkoutis, and H. Y. Hwang, "Superconducting dome in $nd_{1-x}sr_x nio_2$ infinite layer films," Phys. Rev. Lett. **125**, 027001 (2020).

[6] M. Osada, B. Y. Wang, K. Lee, D. Li, and H. Y. Hwang, "Phase diagram of infinite layer praseodymium nickelate $pr_{1-x}sr_x nio_2$ thin films," Phys. Rev. Mater. **4**, 121801 (2020).

[7] S. Zeng, C. Li, L. E. Chow, Y. Cao, Z. Zhang, C. S. Tang, X. Yin, Z. S. Lim, J. Hu, P. Yang, and A. Ariando, "Superconductivity in infinite-layer nickelate $la_{1-x}ca_x nio_2$ thin films," Science Advances **8** (2022), 10.1126/sciadv.abl9927.

[8] S. Zeng, C. S. Tang, X. Yin, C. Li, M. Li, Z. Huang, J. Hu, W. Liu, G. J. Omar, H. Jani, Z. S. Lim, K. Han, D. Wan, P. Yang, S. J. Pennycook, A. T. S. Wee, and A. Ariando, "Phase diagram and superconducting dome of infinite-layer $nd_{1-x}sr_x nio_2$ thin films," Phys. Rev. Lett. **125**, 147003 (2020).

[9] A. S. Botana and M. R. Norman, "Similarities and differences between $lanio_2$ and $cacuo_2$ and implications for superconductivity," Phys. Rev. X **10**, 011024 (2020).

[10] J. F. Mitchell, "A nickelate renaissance," Frontiers in Physics **9** (2021), 10.3389/fphy.2021.813483.

[11] B. H. Goodge, D. Li, K. Lee, M. Osada, B. Y. Wang, G. A. Sawatzky, H. Y. Hwang, and L. F. Kourkoutis, "Doping evolution of the mott–hubbard landscape in infinite-layer nickelates," Proceedings of the National Academy of Sciences **118**, e2007683118 (2021).

[12] M. Hepting, D. Li, C. J. Jia, H. Lu, E. Paris, Y. Tseng, X. Feng, M. Osada, E. Been, Y. Hikita, Y.-D. Chuang, Z. Hussain, K. J. Zhou, A. Nag, M. Garcia-Fernandez, M. Rossi, H. Y. Huang, D. J. Huang, Z. X. Shen, T. Schmitt, H. Y. Hwang, B. Moritz, J. Zaanen, T. P. Devereaux, and W. S. Lee, "Electronic structure of the parent compound of superconducting infinite-layer nickelates," Nature Materials **19**, 381–385 (2020).

[13] M. Kitatani, L. Si, O. Janson, R. Arita, Z. Zhong, and K. Held, "Nickelate superconductors—a renaissance of the one-band Hubbard model," npj Quantum Materials **5**, 59 (2020).

[14] H. Lu, M. Rossi, A. Nag, M. Osada, D. F. Li, K. Lee, B. Y. Wang, M. Garcia-Fernandez, S. Agrestini, Z. X. Shen, E. M. Been, B. Moritz, T. P. Devereaux, J. Zaanen, H. Y. Hwang, Ke-Jin Zhou, and W. S. Lee, "Magnetic excitations in infinite-layer nickelates," Science **373**, 213–216 (2021).

[15] G. Krieger, L. Martinelli, S. Zeng, L. E. Chow, K. Kummer, R. Arpaia, M. Moretti Sala, N. B. Brookes, A. Ariando, N. Viart, M. Salluzzo, G. Ghiringhelli, and D. Preziosi, "Charge and spin order dichotomy in $ndnio_2$ driven by the capping layer," Phys. Rev. Lett. **129**, 027002 (2022).

[16] Tranquada, J. M. and Sternlieb, B. J. and Axe, J. D. and Nakamura, Y. and Uchida, S., "Evidence for stripe correlations of spins and holes in copper oxide superconductors," Nature **375**, 561 (1995).

[17] J. Chang, E. Blackburn, A. T. Holmes, N. B. Christensen, J. Larsen, J. Mesot, Ruixing Liang, D. A. Bonn, W. N. Hardy, A. Watenphul, M. v. Zimmermann, E. M. Forgan, and S. M. Hayden, "Direct observation of competition between superconductivity and charge density wave order in YBa2Cu3O6.67," Nat. Phys. **8**, 871–876 (2012).

[18] G. Ghiringhelli, M. Le Tacon, M. Minola, S. Blanco-Canosa, C. Mazzoli, N. B. Brookes, G. M. De Luca, A. Frano, D. G. Hawthorn, F. He, T. Loew, M. Moretti Sala, D. C. Peets, M. Salluzzo, E. Schierle, R. Sutarto, G. A. Sawatzky, E. Weschke, B. Keimer, and L. Braicovich, "Long-Range Incommensurate Charge Fluctuations in (Y,Nd)Ba2Cu3O6+x," Science **337**, 821–825 (2012).

[19] D. H. da Silva Neto, P. Aynajian, A. Frano, R. Comin, E. Schierle, E. Weschke, A. Gyenis, J. Wen, J. Schneeloch, Z. Xu, S. Ono, G. Gu, M. Le Tacon, and A. Yazdani, "Ubiquitous Interplay Between Charge Ordering and High-Temperature Superconductivity in Cuprates," Science **343**, 393–396 (2014).

[20] H.-C. Jiang and T. P. Devereaux, "Superconductivity in the doped Hubbard model and its interplay with next-nearest hopping t'," Science **365**, 1424–1428 (2019).

[21] V. Marino, F. Becca, and L. F. Tocchio, "Stripes in the extended t-$t\prime$ Hubbard model: A Variational Monte Carlo analysis," SciPost Physics **12**, 180 (2022).

[22] M. Rossi, M. Osada, J. Choi, S. Agrestini, D. Jost, Y. Lee, H. Lu, B. Y. Wang, K. Lee, A. Nag, Y.-D. Chuang, C.-T. Kuo, S.-J. Lee, B. Moritz, T. P. Devereaux, Z.-X. Shen, J.-S. Lee, K.-J. Zhou, H. Y. Hwang, and W.-S. Lee, "A broken translational symmetry state in an infinite-layer nickelate," Nature Physics **18**, 869–873 (2022).

[23] C. C. Tam, J. Choi, X. Ding, S. Agrestini, A. Nag, M. Wu, B. Huang, H. Luo, P. Gao, M. García-Fernández, L. Qiao, and K.-J. Zhou, "Charge density waves in infinite-layer NdNiO2 nickelates," Nature Materials **21**, 1116–1120 (2022).

[24] X. Ren, R. Sutarto, Q. Gao, Q. Wang, J. Li, Y. Wang, T. Xiang, J. Hu, J. Chang, R. Comin, X. J. Zhou, and Z. Zhu, "Two distinct charge orders in infinite-layer PrNiO2+{\delta} revealed by resonant x-ray diffraction," (2024), arXiv:2303.02865 [cond-mat.supr-con].

[25] M. Rossi, H. Lu, K. Lee, B. H. Goodge, J. Choi, M. Osada, Y. Lee, D. Li, B. Y. Wang, D. Jost, S. Agrestini, M. Garcia-Fernandez, Z. X. Shen, Ke-Jin Zhou, E. Been, B. Moritz, L. F. Kourkoutis, T. P. Devereaux, H. Y. Hwang, and W. S. Lee, "Universal orbital and magnetic structures in infinite-layer nickelates," Phys. Rev. B **109**, 024512 (2024).

[26] J. Pelliciari, N. Khan, P. Wasik, A. Barbour, Y. Li, Y. Nie, J. M. Tranquada, V. Bisogni, and C. Mazzoli, "Comment on newly found charge density waves in infinite layer nickelates," (2023), arXiv:2306.15086 [cond-mat.supr-con].

[27] C. T. Parzyck, N. K. Gupta, Y. Wu, V. Anil, L. Bhatt, M. Bouliane, R. Gong, B. Z. Gregory, A. Luo, R. Sutarto, F. He, Y.-D. Chuang, T. Zhou, G. Herranz, L. F. Kourkoutis, A. Singer, D. G. Schlom, D. G. Hawthorn, and K. M. Shen, "Absence of 3a0 charge density wave order in the infinite-layer nickelate NdNiO2," Nature Materials , 1–6 (2024).

[28] L. Si, P. Worm, D. Chen, and K. Held, "Topotactic hydrogen forms chains in abo_2 nickelate superconductors," Phys. Rev. B **107**, 165116 (2023).

[29] A. Raji, G. Krieger, N. Viart, D. Preziosi, J.-P. Rueff, and A. Gloter, "Charge distribution across capped and uncapped infinite-layer neodymium nickelate thin films," Small **19**, 2304872 (2023).

[30] R. Jaramillo, Yejun Feng, J. C. Lang, Z. Islam, G. Srajer, P. B. Littlewood, D. B. McWhan, and T. F. Rosenbaum, "Breakdown of the bardeen–cooper–schrieffer ground state at a quantum phase transition," Nature **459**, 405–409 (2009).

[31] M. v. Zimmermann, J. R. Schneider, T. Frello, N. H. Andersen, J. Madsen, M. Käll, H. F. Poulsen, R. Liang, P. Dosanjh, and W. N. Hardy, "Oxygen-ordering superstructures in underdoped yba2cu3o6+x studied by hard x-ray diffraction," Physical Review B **68**, 104515 (2003).

[32] L. Balents, C. R. Dean, D. K. Efetov, and A. F. Young, "Superconductivity and strong correlations in moiró flat bands," Nature Physics **16**, 725–733 (2020).

[33] M. Osada, B. Y. Wang, B. H. Goodge, K. Lee, H. Yoon, K. Sakuma, D. Li, M. Miura, L. F. Kourkoutis, and H. Y. Hwang, "A superconducting praseodymium nickelate with infinite layer structure," Nano Letters **20**, 5735–5740 (2020), publisher: American Chemical Society.

[34] N. Schell, A. King, F. Beckmann, T. Fischer, M. Müller, and A. Schreyer, "The high energy materials science beamline (hems) at petra iii," Materials Science Forum **772**, 57 – 61 (2010).

[35] J. Gustafson, M. Shipilin, C. Zhang, A. Stierle, U. Hejral, U. Ruett, O. Gutowski, P.-A. Carlsson, M. Skoglundh, and E. Lundgren, "High-energy surface x-ray diffraction for fast surface structure determination," Science **343**, 758–761 (2014).

[36] F. Bertram, O. Gutowski, J. Patommel, C. Schroer, and U. Ruett, "1d silicon refractive lenses for surface scattering with high energy x-rays," AIP Conference Proceedings **1741**, 040003 (2016).
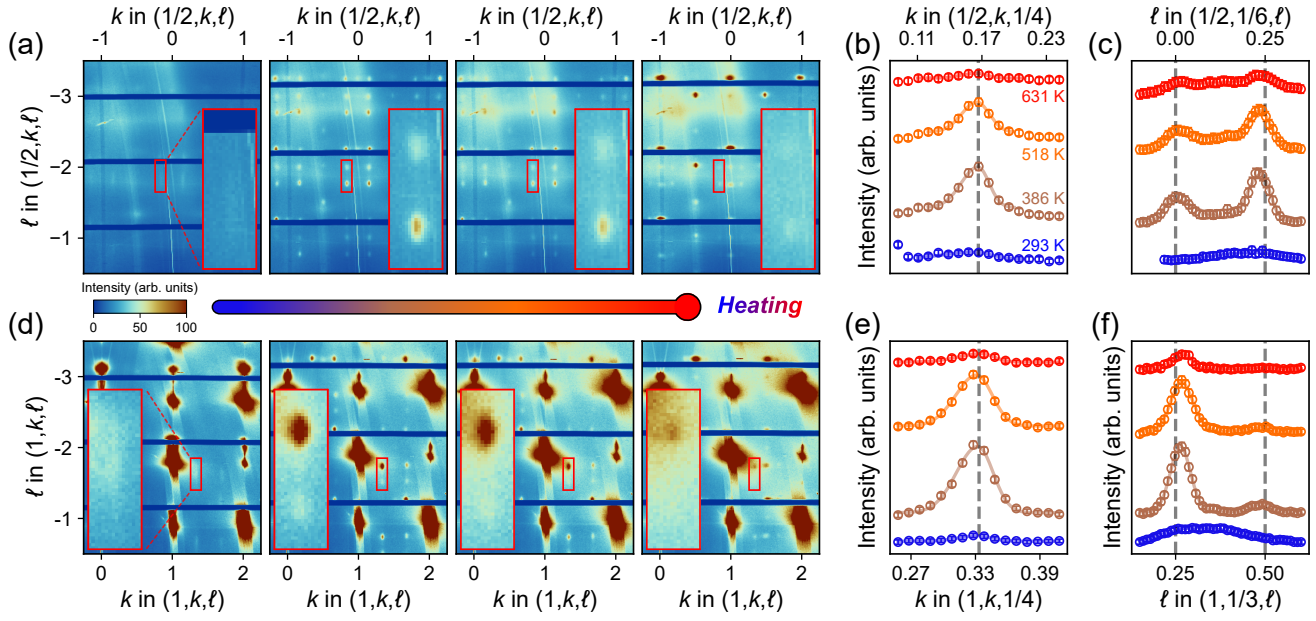
FIG. S1. **Thermal-induced superlattice structure in a PrNiO$_2$ thin film.** (a,d) Diffraction intensities (displayed with a linear false color scale) in the $(1/2, k, \ell)$ and $(1, k, \ell)$ scattering planes as a function of temperature. The most intense peaks stem from fundamental Bragg peaks of the STO substrate and the PrNiO$_2$ thin film. Selected superlattice peaks are highlighted by red rectangular boxes. (b,c,e,f) One-dimensional k (in-plane) and ℓ (out-of-plane) scans through the superlattice reflections for temperatures as indicated. Solid lines are Gaussian profiled fits with a sloping background. Error bars reflect counting statistics.
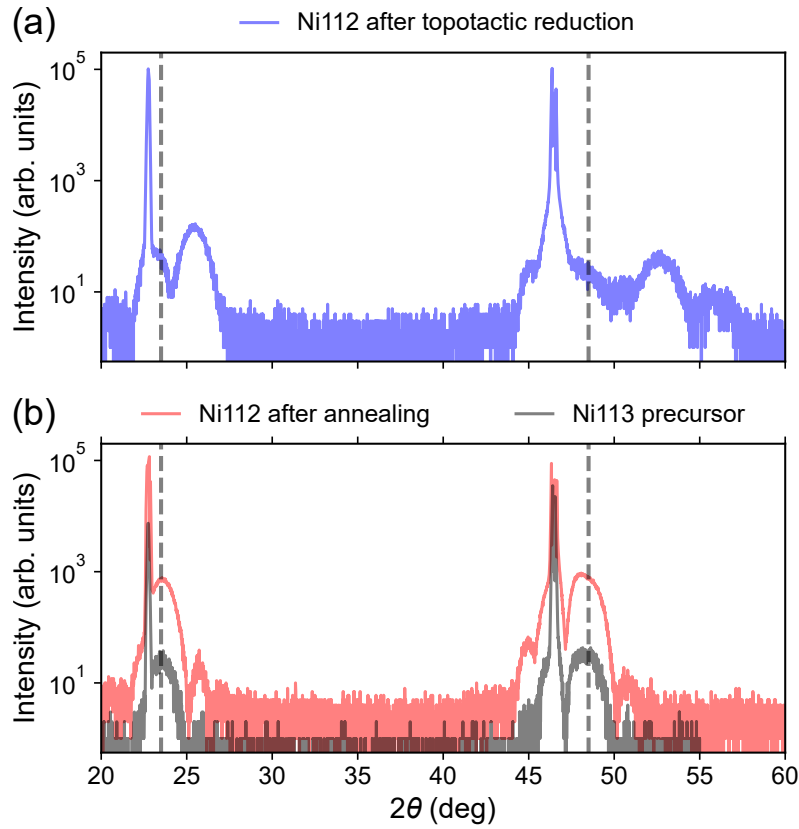
FIG. S2. **Room temperature 2θ scans recorded on PrNiO$_2$ (Ni112) and PrNiO$_3$ thin films with crystalline STO capping layer**. (a) Infinite layer phase Ni112 obtained after topotactic reduction of the perovskite precursor PrNiO$_3$ (Ni113). (b) Comparison of the Ni112 thin film after annealing at high temperatures with the original Ni113 phase. The scans were performed using a SmartLab x-ray diffractometer with a Cu Kα source.
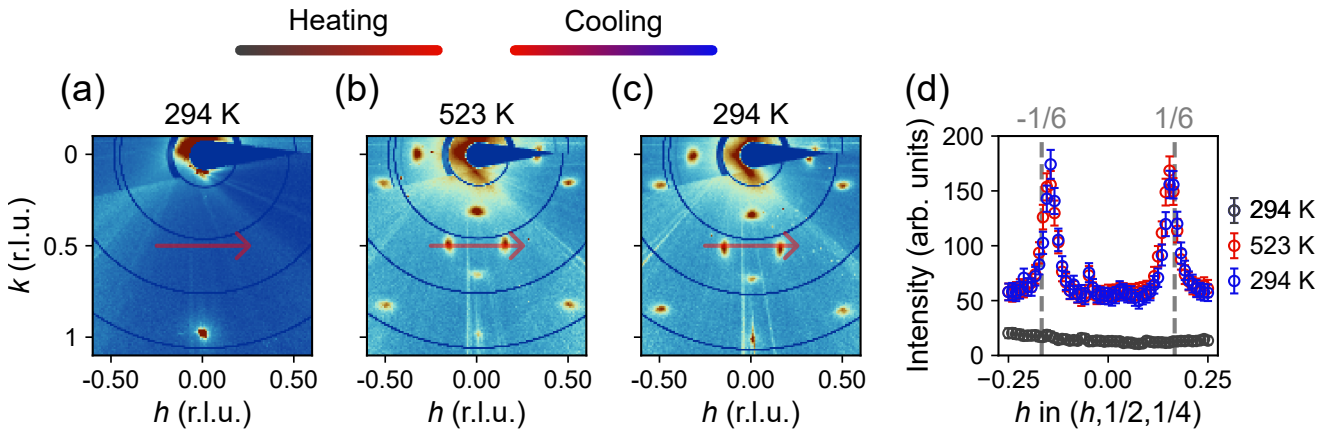
FIG. S3. **Temperature quenching of a PrNiO$_2$ thin film with crystalline STO capping layer**. (a-c) Diffracted intensities within the $(h, k, 1.75)$ scattering plane for temperatures as indicated. (d) Corresponding h-scans through $(h, 1/2, 1/4)$, demonstrating how the annealing-induced symmetry breaking can be quenched. This quenching experiment was carried out on a sample that was kept under vacuum conditions before being introduced into the controlled helium atmosphere in the XRD chamber.